




Unified Surface and Volumetric Inference on Functional Imaging Data

Thomas F. Kirk^{1,2} , Martin S. Craig^{1,2} , and Michael A. Chappell^{1,2} 

¹ Sir Peter Mansfield Imaging Center, School of Medicine, University of Nottingham, Nottingham, UK

tomfrankkirk@gmail.com

² Quantified Imaging, London, UK

<https://physimals.github.io/physimals/>

Abstract. Surface-based analysis methods for functional imaging data have been shown to offer substantial benefits for the study of the human cortex, namely in the localisation of functional areas and the establishment of inter-subject correspondence. A new approach for surface-based parameter estimation via non-linear model fitting on functional time-series data is presented. It treats the different anatomies within the brain in the manner that is most appropriate: surface-based for the cortex, volumetric for white matter, and using regions-of-interest for subcortical grey matter structures. The mapping between these different domains is incorporated using a novel algorithm that accounts for partial volume effects. A variational Bayesian framework is used to perform parameter inference in all anatomies simultaneously rather than separately. This approach, called hybrid inference, has been implemented using stochastic optimisation techniques. A comparison against a conventional volumetric workflow with post-projection on simulated perfusion data reveals improvements parameter recovery, preservation of spatial detail and consistency between spatial resolutions. At 4 mm isotropic resolution, the following improvements were obtained: 2.7% in SSD error of perfusion, 16% in SSD error of Z-score perfusion, and 27% in Bhattacharyya distance of perfusion distribution.

Keywords: surface analysis · neuroimaging · partial volume effect · variational Bayes

1 Introduction

In recent years, there has been increasing interest in performing surface-based analysis of magnetic resonance neuroimaging (MRI) data in the human cortex. A basic assumption that underpins this approach is that cortical activity will correlate better according to geodesic distance (along the surface) than geometric distance (straight-line). The benefits include improvements in the localisation of functional areas and the establishment of inter-subject correspondence [5]. Due to the fact that MRI data is typically acquired on a 3D voxel grid that does not directly correspond with a 2D surface, a necessary pre-processing step is to project the volumetric data onto the cortical surface, a complex operation for

which there is no commonly-agreed upon solution [11, 13]. Of particular relevance is the partial volume effect (PVE): because functional imaging voxels are of comparable size to the thickness of the human cortex, each is likely to contain a mixture of cortical grey matter (GM), white matter (WM) and cerebrospinal fluid (CSF). This mixing of signals from different tissues introduces confound into later analysis steps. Furthermore, because not all anatomies in the brain are amenable to surface analysis, data for the subcortex is usually processed in a volumetric manner. This leads to separate workflows for the different anatomies within the brain, as exemplified by the Human Connectome Project’s (HCP) parallel *fMRISurface* and *fMRIVolume* pipelines [8].

The objective of this work was to develop a framework for parameter inference that is able to operate in a surface and volumetric manner *simultaneously*. This would remove the need for separate workflows whilst ensuring that each anatomy of interest is treated in an optimal manner, namely surface-based for the cortex, volumetric for WM, and region-of-interest (ROI) for subcortical GM structures. This principle corresponds directly with the HCP’s concept of *grayordinates* [8]. In order to achieve this, a novel algorithm that maps data between different representations has been embedded within a modality-specific generative model. Via the use variational Bayesian techniques, it is then possible to perform non-linear model-fitting directly on volumetric timeseries data without pre-processing. The advantages of this approach are demonstrated on simulated perfusion MRI data.

2 Methods

Theory. The spatial locations within the brain at which parameter estimates are obtained are hereafter called *nodes*. A key step in performing inference is to define a mapping between nodes and the voxel data that has been acquired, which is then embedded within a generative model to yield a function that relates physiological parameters to the data they reconstruct. In the case of volumetric inference, this mapping is one-to-one: each node corresponds to exactly one voxel. The concept can be extended to include other types of node: alongside voxels for WM, surface vertices can represent the cortex and volumetric ROIs can represent subcortical GM structures. Collectively these are referred to as *hybrid* nodes, which correspond to grayordinates in the HCP terminology [8]. An illustration is given in Fig. 1.

In this work, the mapping for hybrid nodes previously introduced in [10] was used. It is constructed by calculating the volume of intersection between individual voxels and the geometric primitives that construct the cortical ribbon, WM tracts, or individual ROIs. Importantly, because each node corresponds by definition to exactly one tissue type, the mapping will be many-to-one in voxels that contain multiple tissues which is an explicit representation of PVE. The mapping takes the form of a non-square sparse matrix (number of nodes > voxels), an example of which is illustrated in Fig. 2.

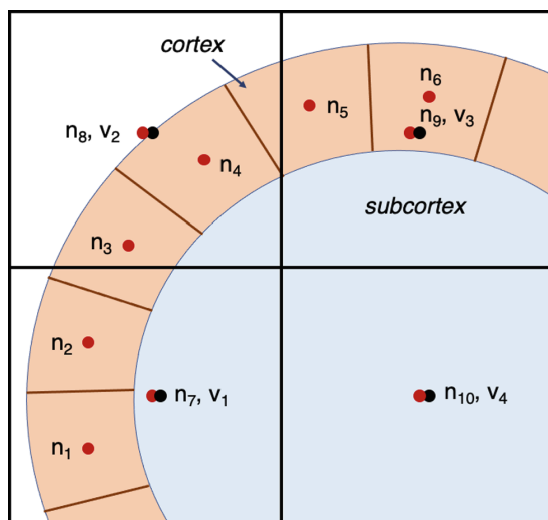


Fig. 1. Simplified representation of voxels and nodes around the cortical ribbon. The voxel grid is shown in black, and voxel centres are labelled v_1 to v_4 . To represent cortical tissue, each volume primitive of the cortex (shaded brown) is assigned a node n_1 to n_6 . For subcortical tissue (shaded blue), each volume primitive is assigned a node n_7 to n_{10} , which correspond exactly to the voxel centres v_1 to v_4 . By definition, each node represents one tissue type. (Color figure online)

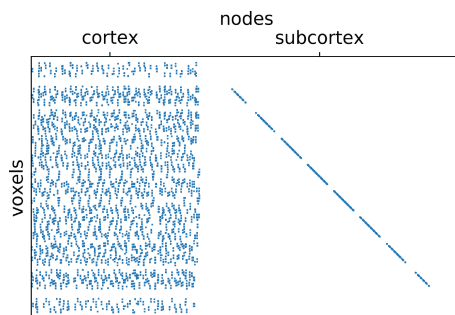


Fig. 2. Sparsity structure of the hybrid node to voxel mapping for a single cortical hemisphere at 32,000 vertex resolution intersecting a 3 mm isotropic voxel grid.

Having defined and embedded the mapping within a generative model, one can turn to the process of parameter inference. We adopt a Bayesian approach because this permits the incorporation of prior knowledge and the quantification of parameter uncertainty. Both attributes are valuable given the challenging signal-to-noise ratio (SNR) of functional imaging data. Under this approach,

the objective is to obtain a posterior distribution p for the parameters θ of a generative model M given observed data y , which may be expressed as:

$$P(\theta|y, M) = \frac{P(y|\theta, M)P(\theta|M)}{P(y|M)} \quad (1)$$

The choice of model M and corresponding physiological parameters θ is determined by the imaging modality in question. In practice, evaluating this expression for all but the most trivial configurations is infeasible due to the integrations entailed (notably the evidence term in the denominator). A number of numerical approaches have thus been developed, one of which is variational Bayes (VB) which approximates the posterior p with an arbitrary distribution q and uses the free energy F to assess the accuracy of approximation [1]. Omitting M from notation, F is defined as:

$$F(\theta) = \int q(\theta) \log \left(p(y|\theta) \frac{p(\theta)}{q(\theta)} \right) d\theta \quad (2)$$

VB thus turns parameter inference into an optimisation problem: *what q best approximates p as measured by the free energy?* One means of implementing this is to use stochastic optimisation techniques. A Monte Carlo approximation to the objective function F may be obtained using an average over L randomly drawn samples θ^{*l} from $q(\theta)$:

$$F \approx \frac{1}{L} \sum_l \left[\log(p(y|\theta^{*l})) - \log \left(\frac{q(\theta^{*l})}{p(\theta^{*l})} \right) \right] \quad (3)$$

This strategy is referred to as stochastic variational Bayes (SVB). By constructing this expression as a computational graph, including the modality-specific generative model M with its embedded mapping from hybrid nodes to voxels, automatic differentiation techniques may be used to maximise F and thus derive the optimal approximation q to the true posterior p . The volumetric implementation of SVB previously introduced in [4] has been extended in this manner and the end result is referred to as hybrid SVB, hSVB. Note that this approach does not involve any learning or training: on each dataset, the inference starts afresh and operates on all data until approximate convergence of the optimisation problem has been reached.

A key advantage of the Bayesian approach is that it enables prior information to be incorporated into the inference. Such priors can either be distributional, for example an empirically-derived normal distribution; or spatial, which encode the belief that parameter values should correlate in adjacent regions of the brain [15]. A spatial prior is particularly useful as a means of mitigating the low SNR inherent to many functional imaging techniques because it applies regularisation in a principled manner that is determined solely by data quality as opposed to relying on user-set parameters. When applied to volumetric data, a drawback of the spatial prior is that it is unaware of underlying anatomy, and in

particular PVE. This is because it is typically implemented using an isotropic Laplacian operator over the first-order neighbourhood of voxels, which is especially problematic at the cortical boundary where it will enforce a similarity constraint across the GM/WM boundary even though these tissues may have different parameter values. Under a hybrid approach, it is possible to restrict the spatial prior to operate only in anatomically contiguous regions. Specifically, one spatial prior is defined on the surface for the cortex, a second spatial prior is defined in the volume for non-cortical tissue, and hence regularisation no longer happens across tissue boundaries. In this work, the isotropic Laplacian on first-order neighbours was used for the volumetric prior, and the discrete cotangent Laplacian was used for the surface prior [6].

Evaluation. hSVB was evaluated using simulated mutli-delay arterial spin labelling (ASL) data, a perfusion modality which is sensitive to both cerebral blood flow (CBF) and arterial transit time (ATT). Inference on multi-delay ASL data requires fitting a non-linear model with two parameters which is more challenging than for single-delay ASL. A single subject’s T1 MPRAGE anatomical image (1.5 mm isotropic resolution, TR 1.9 s, TE 3.74 ms, flip angle 8°) was processed to extract the left cortical hemisphere, which defined the ground truth anatomy from which ASL data was simulated. FreeSurfer was used to obtain mesh reconstructions of the white and pial cortical surfaces [7]; FSL FIRST was used to segment subcortical GM structures [14]; FSL FAST was used to segment cerebrospinal fluid [16]; and finally Toblerone [9] was used to obtain WM PV estimates.

A single-compartment well-mixed ASL model was used to represent term M in Eq. 1 and simulate data [2]. Pseudo-continuous ASL with six post-label delays of [0.25, 0.5, 0.75, 1.0, 1.25, 1.5] s and 1.8 s label duration was used. For the cortex, a ground truth CBF map with a mean value of 60 units and sinusoidal variation of 40 units peak-to-peak was used, illustrated in Fig. 3, and a constant ATT of 1.1 s was used. In WM and subcortical GM structures, constant reference CBF and ATT values were assumed. Data was simulated at spatial resolutions of [2, 3, 4, 5] mm isotropic and SNR levels of $x \cdot 2^n$, $n \in [-1, -0.5, 0, 0.5, 1]$, i.e., from $x/2$ to $2x$, where x represents typical SNR estimated from a single subject’s mutli-delay data acquired in a previous study [12]. In the results, the value x is omitted from notation, so $\text{SNR} = 2^0$ means ‘typical SNR’. This variety of resolutions and SNR levels reflects the diversity of acquisitions seen in clinical practice. In all cases, zero-mean additive white noise was used.

hSVB has been implemented using TensorFlow version 2.9 running on Python 3.9.12. Optimisation was performed using RMSProp with a learning rate of 0.1, a decay factor of 0.97, and a sample size of 10. During training, a reversion to previous best state (‘mean reversion’) was performed when cost did not improve for 50 consecutive epochs; for all experiments, training was run until 20 such reversions had taken place which served as a proxy for convergence. Typically this implied training for around 2000 epochs. A folded normal distribution was used

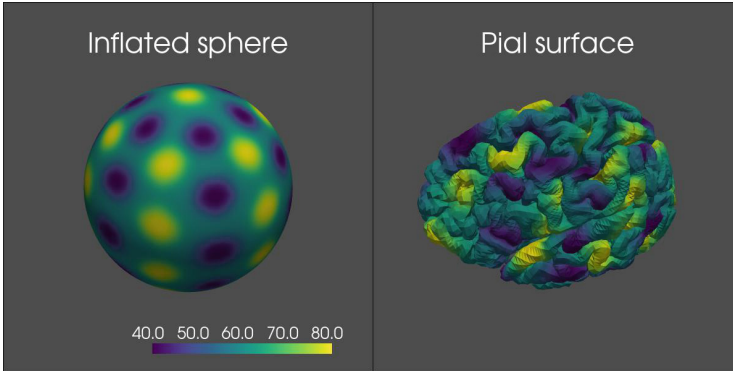


Fig. 3. The ground truth cortical CBF map, illustrated on both the inflated sphere (left) and the native pial surface (right). The signal varies between 40 and 80 units with a mean of 60.

on all model parameters to restrict inference to positive values only. Runtime on a 6 core CPU was around 5 mins per inference, using around 4 GB of RAM.

The comparator method was based on BASIL, a conventional volumetric ASL processing workflow [3]. Specifically, the *oxford_asl* pipeline with partial volume effect correction was run using the same PV estimates from which the ASL data was simulated, and then the GM-specific parameter maps were projected onto the cortical surface using the same method as embedded within hSVB [10]. This method is referred to as BASIL-projected, BP. Runtime (single-threaded) was around 5 min per inference, using around 1 GB of RAM.

Performance was assessed by calculating the following metrics with respect to the ground truth cortical CBF map: sum of squared differences (SSD) of CBF; SSD of Z-transformed CBF, and Bhattacharyya distance of CBF distribution. The second and third metrics are included because they are sensitive to relative perfusion, whereas the first is sensitive to absolute CBF. A receiver-operator characteristic (ROC) analysis was performed using a binary classifier of varying threshold value t . Recalling that the ground truth CBF map had a mean value of 60 with extrema of ± 20 , t was set at values of 5 to 15 with an increment of 1. At each t , areas of hypoperfusion were classified with a threshold value of $60 - t$ and hyperperfusion with $60 + t$. The area-under ROC (AUROC) for hypo and hyperperfusion was then calculated and the mean of the two taken. This yielded an AUROC score for each method at varying levels of threshold t .

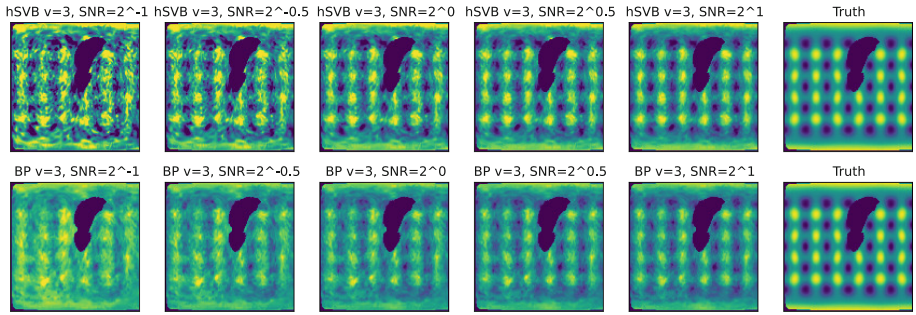


Fig. 4. Cortical CBF maps estimated from 3 mm data. Each map has been flattened onto a 2D plane for visual inspection. The blank spot corresponds to the corpus callosum which has no defined cortical thickness and therefore does not support parameter estimation.

3 Results

Figure 4 shows cortical CBF maps estimated by both methods on 3 mm data, flattened down onto a 2D plane for ease of inspection. For all SNR, hSVB’s map retained more contrast than BP’s: the bright spots were brighter, and vice-versa, particularly so at low SNR. At $\text{SNR} = 2^{-1}$, BP’s result displayed a positive bias in CBF which was readily observed by comparison to other SNR levels.

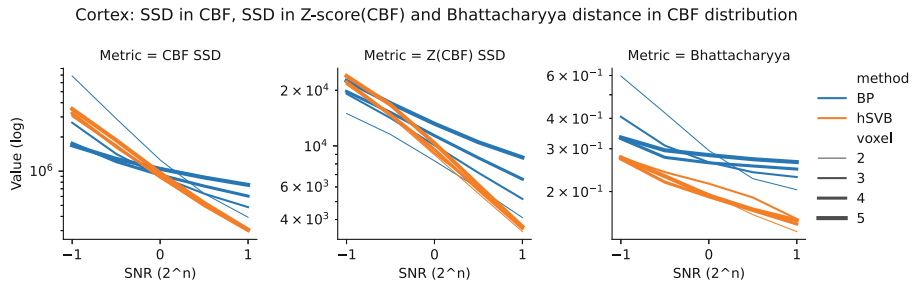


Fig. 5. SSD in CBF, SSD in Z-transformed CBF, and Bhattacharyya distance in CBF perfusion distribution, all evaluated for the cortex. Note in all panels the greater consistency in hSVB’s scores across voxel sizes compared to BP.

Figure 5 shows SSD in CBF, SSD in Z-transformed CBF, and Bhattacharyya distance of CBF perfusion distribution, all for the cortex. For SSD, hSVB performed worse than BP at low SNR, and better for $\text{SNR} \geq 2^0$. By contrast, for SSD of Z-transformed CBF, hSVB performed better at almost all SNR. In Bhattacharyya distance, hSVB performed better at all voxel sizes and SNR. Of note in all panels was the consistency of hSVB’s results across voxel sizes, whereas BP

displayed greater variation (particularly for SSD of Z-transformed CBF, where the 2 mm result was substantially better than all others).

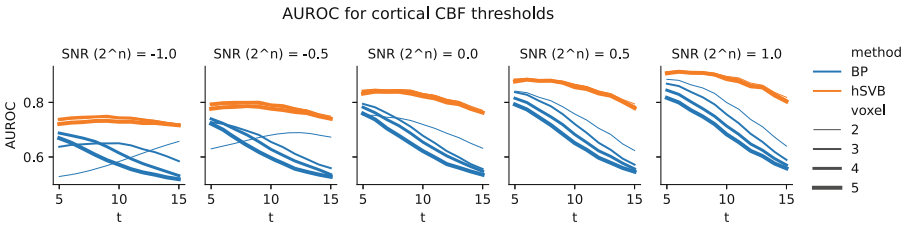


Fig. 6. AUROC scores for binary classification of cortical hypo and hyper-perfusion at varying threshold values t . For all comparisons, hSVB obtained a higher score than BP.

Figure 6 shows AUROC scores for binary classification of the estimated CBF maps returned by both methods. For all voxel sizes and SNR, the AUROC score for hSVB was higher than that of BP, particularly at high threshold values.

4 Discussion

The results presented here demonstrate that a hybrid approach to parameter inference using SVB (hSVB) offers a compelling alternative for the surface-based analysis of functional neuroimaging data. hSVB can operate directly on volumetric data without pre-processing and is able to apply the spatial prior in an anatomically-informed manner that respects tissue boundaries.

Applied to simulated ASL data, hSVB demonstrated a number of positive attributes in relation to a conventional volumetric workflow with post-projection (BP). Firstly, greater consistency in performance across voxel sizes was observed. As spatial resolution directly determines the extent of PVE within data, this implied that hSVB is more robust to PVE which is an important source of confound. Secondly, at higher levels of SNR, hSVB was able to deliver estimates that scored substantially better across a variety of metrics, which suggests it is well-placed to exploit future increases in SNR that result from advances in hardware and acquisition. Finally, hSVB was better able to discern relative perfusion differences, i.e., areas of abnormality. The trade-off for this was higher SSD errors in absolute perfusion values at low SNR.

A key point of divergence between hSVB and BP observed in this work was in the effect of the spatial prior at low SNR levels. Bayesian inference can be understood as an updating process whereby the prior distribution is modified to the extent that the observed data supports this. For low SNR data, the data will support less deviation from the priors. Referring to Fig. 4, BP tended towards globally homogenous solutions with high smoothing and low detail, whereas hSVB did the opposite: increasingly heterogenous ('textured', in the language

of image analysis) solutions with low smoothing and high detail. In this scenario, the SSD of CBF metric is asymmetric: as smoothing increases towards a perfectly homogenous solution, SSD will approach a finite asymptotic value, whereas in the opposite outcome of increasingly extreme minima and maxima that preserve overall detail, SSD will increase towards infinity. It is believed that this mechanism explains the high SSD errors obtained by hSVB at low SNR, and also explains why hSVB performed much better on a relative basis (SSD of Z-score CBF), where the ability to distinguish perfusion variation matters more than the absolute values.

Two limitations of this work are that the ground truth cortical CBF map used to simulate data (Fig. 3) is clearly highly contrived, and the simulation did not include any of the imperfections normally seen in acquisition data, such as motion, intensity or geometric distortion artefacts. Though such problems are normally dealt with prior to performing inference via separate pre-processing operations, they can rarely be fully corrected, and thus some residual artefact may remain during inference which may degrade performance. The next step in the development of this work will be to try hSVB on human acquisition data to verify similar performance to the results presented here, which is currently in progress.

References

1. Attias, H.: A variational Bayesian framework for graphical models. In: *Advances in Neural Information Processing Systems*, pp. 209–215 (2000). ISBN 0262194503
2. Buxton, R.B., Frank, L.R., Wong, E.C., Siewert, B., Warach, S., Edelman, R.R.: A general kinetic model for quantitative perfusion imaging with arterial spin labeling. *Magn. Reson. Med.* **40**(3), 383–396 (1998). <https://doi.org/10.1002/mrm.1910400308>. ISBN 1522-2594
3. Chappell, M., Groves, A., Whitcher, B., Woolrich, M.: Variational Bayesian inference for a nonlinear forward model. *IEEE Trans. Signal Process.* **57**(1), 223–236 (2009). <https://doi.org/10.1109/TSP.2008.2005752>. ISBN 1053-587X
4. Chappell, M.A., Craig, M.S., Woolrich, M.W.: Stochastic variational Bayesian inference for a nonlinear forward model. *arXiv e-prints* [arXiv:2007.01675](https://arxiv.org/abs/2007.01675) (2020). *arXiv, eess.SP/2007.01675*
5. Coalson, T.S., Van Essen, D.C., Glasser, M.F.: Lost in Space: The Impact of Traditional Neuroimaging Methods on the Spatial Localization of Cortical Areas. *bioRxiv*, p. 255620 (2018). Publisher: Cold Spring Harbor Laboratory
6. Desbrun, M., Meyer, M., Schröder, P., Barr, A.H.: Implicit fairing of irregular meshes using diffusion and curvature flow. In: *Proceedings of the 26th Annual Conference on Computer Graphics and Interactive Techniques, SIGGRAPH 1999*, pp. 317–324. ACM Press (1999). <https://doi.org/10.1145/311535.311576>. <http://portal.acm.org/citation.cfm?doid=311535.311576>
7. Fischl, B.: FreeSurfer. *Neuroimage* **62**(2), 774–781 (2012). <https://doi.org/10.1016/j.neuroimage.2012.01.021.FreeSurfer>. [arXiv:0905.26710](https://arxiv.org/abs/0905.26710). ISBN 1095-9572 (Electronic) 0053-8119 (Linking)

8. Glasser, M.F., et al.: The minimal preprocessing pipelines for the Human Connectome Project. *NeuroImage* **80**, 105–124 (2013). <https://doi.org/10.1016/j.neuroimage.2013.04.127>. arXiv, NIHMS150003. Publisher: Elsevier Inc. ISBN 1053-8119
9. Kirk, T.F., Coalson, T.S., Craig, M.S., Chappell, M.A.: Toblerone: surface-based partial volume estimation. *IEEE Trans. Med. Imaging* **39**(5), 1501–1510 (2020). <https://doi.org/10.1109/TMI.2019.2951080>
10. Kirk, T.F., Craig, M.S., Chappell, M.A.: Unified surface and volumetric projection of physiological imaging data (2022). <https://doi.org/10.1101/2022.01.28.477071>. <https://www.biorxiv.org/content/10.1101/2022.01.28.477071v1>, p. 2022.01.28.477071 Section: New Results
11. Lonjaret, L.T., Bakhous, C., Boutelier, T., Takerkart, S., Coulon, O.: ISA - an inverse surface-based approach for cortical fMRI data projection. In: 14th IEEE International Symposium on Biomedical Imaging, ISBI 2017, Melbourne, Australia, 18–21 April 2017, pp. 1104–1107. IEEE (2017). <https://doi.org/10.1109/ISBI.2017.7950709>
12. Mezue, M., Segerdahl, A.R., Okell, T.W., Chappell, M.A., Kelly, M.E., Tracey, I.: Optimization and reliability of multiple postlabeling delay pseudo-continuous arterial spin labeling during rest and stimulus-induced functional task activation. *J. Cerebral Blood Flow Metab.* **34**(12), 1919–1927 (2014). <https://doi.org/10.1038/jcbfm.2014.163>. <https://www.ncbi.nlm.nih.gov/pubmed/25269517>. Publisher: Nature Publishing Group
13. Operto, G., Bulot, R., Anton, J.L., Coulon, O.: Projection of fMRI data onto the cortical surface using anatomically-informed convolution kernels. *NeuroImage* **39**(1), 127–135 (2008). <https://doi.org/10.1016/j.neuroimage.2007.08.039>. <http://linkinghub.elsevier.com/retrieve/pii/S1053811907007586>
14. Patenaude, B., Smith, S.M., Kennedy, D.N., Jenkinson, M.: A Bayesian model of shape and appearance for subcortical brain segmentation. *NeuroImage* **56**(3), 907–922 (2011). <https://doi.org/10.1016/J.NEUROIMAGE.2011.02.046>. <https://www.sciencedirect.com/science/article/pii/S1053811911002023>. Publisher: Academic Press
15. Penny, W.D., Trujillo-Barreto, N.J., Friston, K.J.: Bayesian fMRI time series analysis with spatial priors. *Neuroimage* **24**(2), 350–362 (2005). <https://doi.org/10.1016/j.neuroimage.2004.08.034>
16. Zhang, Y., Brady, M., Smith, S.: Segmentation of brain MR images through a hidden Markov random field model and the expectation-maximization algorithm. *IEEE Trans. Med. Imaging* **20**(1), 45–57 (2001). <https://doi.org/10.1109/42.906424>. ISBN 0278-0062 (Print) 0278-0062 (Linking)